METHODS AND ANALYSES FOR EVALUATION OF EROSIVE BURNING IN SOLID PROPELLANTS

by

Timothy Charles Wagner

Thesis submitted to the Faculty of the
Virginia Polytechnic Institute and State University
in partial fulfillment of the requirements for the degree of

MASTER OF SCIENCE
in
Mechanical Engineering

APPROVED:

Walter F. O'Brien, Chairman

Henry L. Wood

Eugene F. Brown

April, 1983
Blacksburg, Virginia

METHODS AND ANALYSES FOR EVALUATION OF EROSIVE BURNING IN SOLID PROPELLANTS

by

Timothy C. Wagner

(ABSTRACT)

This investigation was concerned with the measurement and prediction of erosive burning. The theoretical models for erosive burning in composite propellants were reviewed. The experimental techniques which were cited in the literature for the measurement of erosive burning were also reviewed. Only the high-speed motion picture technique was found to have resolution sufficiently high to measure erosive burning accurately. The theory for the microwave burning rate measurement technique was also presented. Although this technique has never been applied to the measurement of erosive burning, it has high resolution and does not interfere with the internal flow over the propellant. For these reasons, microwave interferometry was recommended as the experimental method best suited to measure erosive burning.

Utilizing the microwave technique, a preliminary design for an erosive burning tester was proposed. The proposed apparatus could generate crossflows from Mach 0.2

to Mach 1.0 over the propellant in the test section. A preliminary test plan for verifying the microwave measurement technique was presented.

ACKNOWLEDGMENTS

I owe my deepest thanks to Dr. W. F. O'Brien, my major professor, and Dr. H. L. Wood, co-investigator on this project. Their guidance and encouragement have made working on this project a pleasure.

I also want to thank the Naval Ordnance Station of Indian Head, Maryland, for their support of this project.

Finally, I would like to express a special thanks to my family for their love and support.

TABLE OF CONTENTS

LIST OF FIGURES

NOMENCLATURE

a	Constant in Lenoir and Robillard equation
a_w	Distance between the reference position and the fixed reflection
A	Flow area over propellant
A_b	Burning surface area of solid propellant
A_e	Area at exit
$Amp(t)$	Amplitude output of phase-gain measuring device
A_s	Arrhenius frequency factor
b	Propellant web thickness
B	Injection strength parameter
C_P	Heat capacity of combustion gases
C_{P_b}	Heat capacity of solid propellant
d	Diameter of grain port
D	Oxidizer particle diameter
E_{as}	Activation energy in the propellant surface decomposition
E_o	Magnitude of the incident signal
F	Blowing rate (equation 2.1)
F	Thrust
F_d	Oxidizer distribution function
G	Mass velocity of combustion gas
$GAIN$	External gain of phase-gain measuring device
h	Initial distance between top surface of propellant and chamber
j	$\sqrt{-1}$

k	Specific heat ratio
k_P	Intrinsic wave constant for propagation in unbounded propellant
k_w	Intrinsic wave constant for propagation in air filled waveguide
$\ell(t)$	Instantaneous length of the propellant
ℓ_H	Effective length of the microwave horn.
L	Length from head end of grain.
L_p	Initial length of propellant
m	Mass flow rate
M	Mach number
MW	Molecular weight
n	Exponent in turbulent boundary layer velocity profile (equation 3.4a)
n	Exponential constant
P	Pressure
P_e	Pressure at exit
P_r	Prandtl number of combustion gases
P_o	Chamber pressure (driver motor pressure)
P_3	Atmospheric pressure
Q	Heat required to heat the propellant to the surface temperature and to transform it into gases
r	Total burning rate of the solid propellant
r_d	Total burning rate of a pseudopropellant
r_e	Erosive burning rate
r_o	Normal (strand) burning rate

r_o^*	Linear burning rate
r_p	Plateau burning rate
Re_x	Longitudinal Reynolds number
R_u	Universal Gas Constant
t	Time
t_f	Time of burnout
T	Absolute temperature
T_A	Transmission coefficient for propagation in the incident direction
T_A'	Transmission coefficient for propagation opposite the incident direction
T_f	Flame temperature
T_i	Ambient propellant temperature
T_s	Propellant surface temperature
T_t	Throat temperature
T_o	Chamber temperature (driver motor temperature)
u_∞	Free stream velocity
V	Velocity
V_A	Signal representing the sum of the fixed reflections
V_b	Velocity of gases at burnout
$V_B(t)$	Burning surface reflection signal
$V_c(t)$	Resultant signal
V_D	Velocity resulting from combustion in the driver motor
V_e	Velocity at exit
V_I	Incident signal

V_P	Velocity resulting from combustion of propellant in test section
V_R	Reference signal
V_1	Reflected signal from the air - material 1 interface
V_2	Reflected signal from the material 1 - material 2 interface
V_3	Reflected signal from the material 2 - propellant interface
$\|V_A\|$	Magnitude of fixed reflections
$\|V_B(t)\|$	Magnitude of burning surface signal
$\|V_c(t)\|$	Magnitude of resultant signal
$\|V_A\|_{cf}$	Coefficient of V_A, equivalent to V_A
$\|V_B\|_{cf}$	Coefficient of $V_B(t)$
XNULL	Internal gain of phase-gain measuring device
α	Exponent in turbulent velocity profile (equation 3.4b)
α	Erosive constant in Lenoir and Robillard equation
α_d	Oxidizer mass fraction of a pseudopropellant
α_H	Effective attenuation constant of the microwave horn
α_P	Attenuation constant of the propellant
β	Dimensionless exponential constant
γ	Parameter in plateau burning rate law
Γ_A	Reflection coefficient of the fixed reflection
Γ_B	Reflection coefficient of the burning surface
δ	Boundary layer thickness
δ_2	Momentum thickness of boundary layer

λ_p	Wavelength of microwaves in unbounded propellant
μ	Viscosity of combustion gases
ν	Kinematic viscosity
ρ	Density
ρ_b	Density of solid propellant
ρ_D	Density of gases evolving from the driver motor
ρ_p	Density of gases evolving from propellant in test section
$(\rho u)_w$	Mass flux per unit area of gas evolved from the surface
$(\rho u)_s$	Main stream mass flux across the surface
Φ_a	Angular position of $V_B(t)$ relative to the fixed reference signal
Φ_m	Angular position of $V_c(t)$ relative to the fixed reference signal
$\emptyset_A$	Phase shift due to a signal reflecting from the fixed interface
$\emptyset'_A$	Sum of reflection phase shifts resulting from the path length phase shift and the fixed reflection interface phase jump
$\emptyset_B$	Phase shift due to a signal reflecting from the burning surface
$\emptyset'_B$	Sum of reflection phase shifts resulting from the path length phase shift and the burning surface reflection
Ψ	Function expressing the blocking effect of injection

Section 1

INTRODUCTION

In the design of a solid propellant rocket motor, a continuous knowledge of the burning rate of the propellant at all locations inside the motor is crucial. The burning rate may be affected by high velocity crossflow, changes in chamber pressure, nonhomogeneity of the propellant, and other phenomena. Of these factors, erosive burning, the increase in the normal burning rate due to high velocity crossflow, is probably the most difficult to predict. The designer needs to know the sensitivity of a propellant to erosive burning and be able to accurately predict the amount of erosive burning which will occur in a rocket motor. Failure to do so could result in bursting the case from over-pressurization, or at least altering the expected performance.

Several techniques exist to predict erosive burning but no general theory has gained wide acceptance. More data is needed to evaluate the techniques and develop a comprehensive theory. In order to be useful, continuous burning rate measurements must be made under erosive burning conditions. Of the methods available, the microwave

technique is the only one which provides accurate continuous data without disrupting the internal flow.

After reviewing the current techniques for predicting and measuring erosive burning, the microwave measuring technique will be explained. A preliminary design of an erosive burning tester utilizing the microwave measuring technique will then be presented. The rocket test facilities at VPI&SU will also be described. Finally, the plans for a slab burner to initially test the microwave technique will be presented.

Section 2

REVIEW OF EROSIVE BURNING RESEARCH

The subject of erosive burning has been studied by many investigators in the last thirty years. Literature reviews on the subject have been published by King [1]* and Kuo and Razdan [2]. This review of erosive burning will summarize both the proposed theoretical models and the experimental techniques used to measure erosive burning. The theoretical review will be limited to models for composite propellants.

2.1 EROSIVE BURNING MODELS

In his literature review, King [1] divided the existing theories of erosive burning into four categories:

1. Models based on heat transfer from a "core gas" in the presence of crossflow,
2. Models based on alteration of transport properties in region from surface to flame zone by crossflow, generally due to turbulence effects. Includes effects on conductivity from flame zone back to propellant and effects on time for consumption of fuel pockets leaving surface,
3. Models based on chemically reacting boundary-layer theory, and
4. Other.

---

*Numbers in brackets refer to references listed in the Bibliography.

This review will utilize these categories.

The first category involves those models which are based on heat transfer theory only and ignore the details of combustion. The theory of Lenoir and Robillard [3] is in this category. This burning rate law, one of the first theories in this field, is still the most often-used model for erosive burning. Lenoir and Robillard assumed that the burning rate is the sum of the normal (no crossflow) burning rate, which is dependent on pressure, and the erosive burning rate, which is assumed to be proportional to the heat transfer coefficient.

Many modifications to the Lenoir and Robillard theory have been proposed. Both Matthew and Lawrence [4] and Yamada, Goto, and Ishikawa [5] found better agreement with experiment by using the grain port diameter in place of a length parameter. Jojic and Blagojevic [6] broadened the Lenoir and Robillard theory to account for the decrease in burning rate sometimes found at the head end of the grain. This phenomenon is known as negative erosion. One final modification, proposed by King [7], allowed the normal burning rate to be affected by the crossflow.

The second category used by King is composed of models based on the augmentation of transport properties in the region between the flame zone and the propellant surface. The two most advanced models for composite propellants in

this category are those of Lengelle and of Renie and Osborn.

Lengelle [8] modifies the Granular Diffusion Flame (GDF) Model to allow for turbulent transport coefficients in the gas phase reaction zone. An integral solution is used to solve the turbulent boundary layer equations. The result is an additive law which combines the normal burning rate with an erosive term dependent on pressure and velocity.

The model proposed by Renie and Osborn [9, 10] utilizes the Petite Ensemble Model (PEM) of steady state combustion. The PEM is a statistical model that allows the oxidizer particles to have a distributed size rather than one given diameter. The burning rate is then a statistical summation process over all the oxidizer particle diameters. In order to solve for the erosive burning rate, Renie and Osborn combined the PEM with a velocity profile in an iterative solution.

The third category, models based on chemically reacting boundary layer theory, has only one primary set of contributors for composite propellants, Kuo and Razdan [11 - 14]. These two investigators have developed a model for erosive burning which utilizes a second order closure technique. The governing equations are derived from the conservation equations for a reacting compressible fluid.

The heterogeneous nature of the chemical reactions is included through the eddy-breakup model (EBM) of Spalding. Kuo and Razdan have also extended their model for the case of axisymmetric flow [14].

The fourth category used by King consists of theories which are not covered by the first three categories. Included are models proposed by Parkinson, Klimov, and King.

Parkinson [15, 16] developed a theory to predict pressure-time histories of motors subject to erosive burning based on a "blow-off" phenomenon. The assumption is that when no erosion is present, the transpiring gases have forced the boundary layer away from the surface of the propellant. The boundary layer in this situation is referred to as having been "blown off" the surface. When high crossflow is present, Parkinson suggests that the boundary layer reattaches and erosive burning begins.

Klimov [17] has presented a theory similar to that of Parkinson. However, Klimov goes on to suggest that negative erosion is the result of a "stirring up" of the cool binder decomposition products. These products, being cooler than the oxidizer vapors, act to screen the surface from part of the heat flux generated by the diffusion flame.

The third miscellaneous model for composite propellants is that of King [18 - 21]. King's model is based on a modification of the Beckstead-Derr-Price (BDP) model of combustion of solid propellants [19]. King proposes that erosive burning results from an increase in heat transfer between the heat release zone and the propellant surface due to a combination of turbulence effects and the bending of columnar diffusion flames. The turbulence augments the transport properties between the flame and the surface, while the bending of the diffusion flames brings the heat release zone closer to the propellant surface.

Before leaving the review of erosive burning theories, a few observations will be listed which are cited in the literature and which have special significance to the present investigation.

1. Parkinson [15] noted that 250 motor firings correlated fairly well when plotted as the ratio of maximum to minimum pressure versus blowing rate, F, times the Reynolds number raised to the 0.2 power. The blowing rate is defined as

$$F = \frac{(\rho u)_w}{(\rho u)_s} \tag{2.1}$$

where $(\rho u)_w$ = mass flux per unit area of gas evolved from the surface

$(\rho u)_s$ = main stream mass flux across the surface

This observation is interesting because the 250 motors differed in size, grain design, and type of propellant. (Some of the motors had double base propellant while others were composite). This observation led Parkinson to suggest that erosive burning is a fluid dynamic phenomenon.

2. Several investigators [4, 5, 22] have pointed out that adding aluminum to a propellant does not alter its erosive burning characteristics.
3. Kuo and Razdan [11] consider surface roughness to be an important factor in erosive burning.

2.2 EXPERIMENTAL METHODS

Various techniques have been employed to measure erosive burning experimentally. Some methods are simulative in nature while others attempt to measure a burning propellant under erosive conditions. Five different techniques for obtaining actual measurements will be reviewed here along with one simulative study.

Several investigators [3, 4, 23] have measured erosive burning using the interrupted burning technique. In this method the combustion is interrupted by rapid depressurization and/or purging of the chamber with an inert gas. The burning rate is calculated by dividing the change in

thickness of the propellant by the elapsed time. This method, although frequently used, results in only average burning rates with low accuracy.

Marklund and Lake [22] tried two different experimental methods to measure erosive burning. One method was the x-ray flash technique. At a known time after ignition, an x-ray picture was made of the burning propellant. After measuring the difference in thickness between the original propellant and the image of the propellant on the negative, the burning rate could be calculated as it was using interrupted burning. The second method consisted of two pieces of propellant, each with a pressure transducer embedded at a different depth. As the propellant receded past the inlets to the transducers, two pressure spikes were recorded at different times. Knowing the thickness of the propellants covering the transducers and the two burn times, the burning rate could be calculated. Sturm and Reichenbach [24], in their study of the effects of acceleration on erosive burning, used a similar method, except that the pressure transducers were replaced with timing wires. All of these methods yield only average burning rates with low accuracy.

Photography is the fourth technique that has been used to measure erosive burning. The combustion process is recorded on film using a high-speed motion picture camera

through a glass or quartz window. The camera records both the burning propellant and a timing mark, which is all of the information necessary for the calculation of the burning rate. This method, which has been used by King [20] and Kuo and Razdan [12, 13], yields instantaneous burning rates with good accuracy for the propellant immediately inside the window visible to the camera.

The only experimental technique reported in the literature which is applicable to full scale motors, yet does not disrupt the internal flow, is the method of deducing the burning rate from the pressure-time history. Parkinson [15, 16] has worked on this concept, although his approach is to predict the pressure time history and compare that to the results of a test firing. Based on his boundary layer theory, Parkinson has written a computer code which calculates the erosive burning expected and then generates a predicted pressure time history. Use of this method does not result in a measured value of burning rate. Instead, the result is a predicted burning rate which, when combined with the assumed internal flow, correctly predicts the measured pressure-time history.

One simulative study, done by Yamada, Goto and Ishikawa [5], used porous walls and ambient air to characterize the flow field of a rocket motor under erosive conditions. The results showed that the boundary layer

along the propellant develops rapidly in a manner similar to pipe flow. It was this finding that led these investigators to recommend the use of a pipe diameter in place of a length parameter in the Lenoir and Robillard theory.

Section 3

DISCUSSION OF EROSIVE BURNING MODELS AND EXPERIMENTAL TECHNIQUES

While the previous section was devoted to a review of the literature, this section will present a discussion of the models for erosive burning and the experimental techniques which have been used. The equations for some of the models will be presented for comparison. King's four categories will once again be used.

Before proceeding with the discussion, a list of general observations about erosive burning, compiled by Kuo and Razdan [2], will be given.

Threshold Velocity. It has been observed that the burning rate of solid propellant increases only when the velocity of combustion gases or mass velocity has a value greater than a threshold value. Threshold velocity has been observed to be a function of pressure.

Negative Erosion. At low velocities (below the threshold value) many investigators have reported a decrease in the burning rate compared to the normal burning rate.

Effect of Propellant Initial Temperature. An increase in the erosive burning effect due to a decrease in the propellant initial temperature has been observed.

Effect of Gas Temperature. At constant gas velocity and pressure, the erosive burning rate is found to be independent of the gas temperature.

Effect of Pressure. For a given mass-velocity, erosion is more pronounced under lower pressures. The influence of type of fuel and mixture ratio on the erosive burning diminishes for high pressures.

Effect of Compressibility of the Gaseous Stream. Erosive burning has been found to depend upon the Mach number of the convective stream.

Effect of Burning Rate. Low burning rate propellants have been found to experience larger erosion than fast burning propellants, and vice versa. For high burning rate propellants, pronounced threshold velocity and strong influence of gas mass velocity on erosive burning rate have been observed.

Effect of Propellant Characteristics. Erosive burning has been found to be strongly dependent on the type of binder, fuel and the mixture ratio used.

Effect of Metal Addition. Very little effect on erosive burning by the addition of aluminum has been found.

3.1 DISCUSSION OF EROSIVE BURNING MODELS

Category 1

Models based solely on heat transfer form the first category. These include the theory of Lenoir and Robillard and several modifications. Using empirical expressions for turbulent flow with transpiration, Lenoir and Robillard [3] developed the following expression for the burning rate, r:

$$r = aP^n + \alpha G^{0.8} L^{-0.2} \exp(-\beta \rho_b r/G) \tag{3.1a}$$

where

$$\alpha = 0.0288 \, C_p{}_\mu{}^{0.2} \, Pr^{-0.667} \left[\frac{T_f - T_s}{\rho_b C_{P_b} (T_s - T_i)} \right] \tag{3.1b}$$

Matthews and Lawrence [4] and Yamada, Goto, and Ishikawa [5] both proposed the same modifications to this theory. Their modified burning rate equation is identical to the Lenoir and Robillard expression except that the length, L, is replaced with the port diameter, d.

Jojic and Blagojevic [6] have proposed a modification to the Lenoir and Robillard equation which attempts to account for negative erosion. Jojic and Blagojevic begin by noting that many propellants in use today have a plateau effect: that is, a pressure region where the exponent, n, is zero. A logarithmic plot of burning rate versus pressure for such a propellant is presented in Fig. 1. The variable, r_o^*, represents the burning rate for the pressure

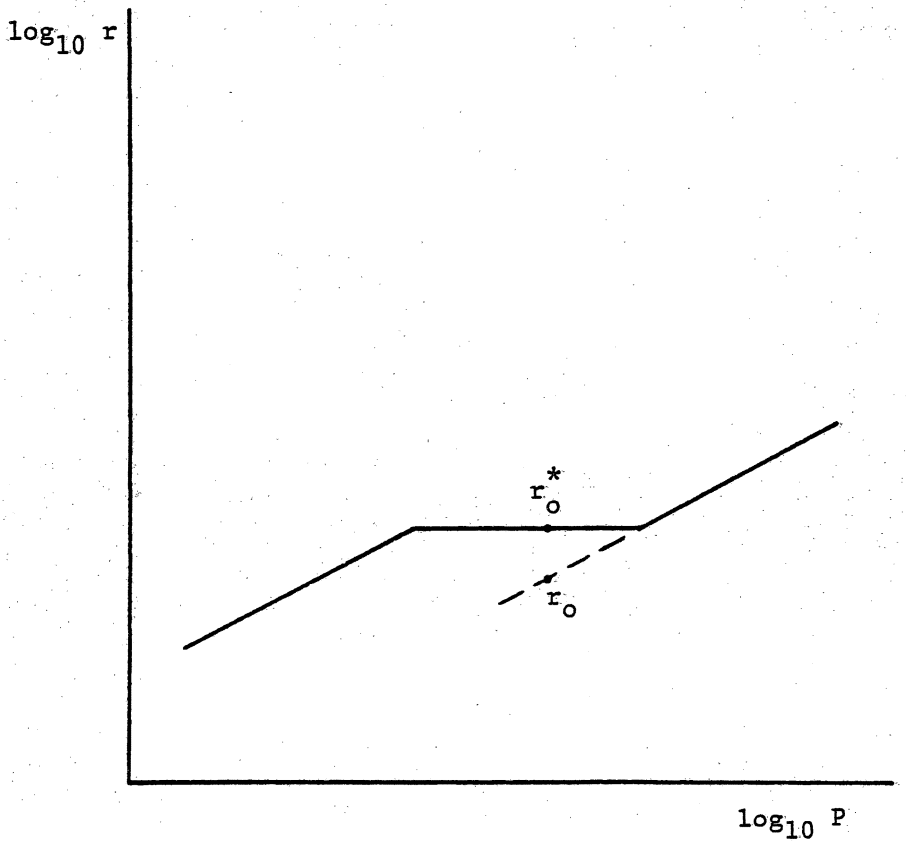

Figure 1. Burning Rate Versus Pressure for a Plateau Propellant [6].

range in which the burning rate is almost constant. Assuming that the plateau effect is altered by crossflow, Jojic and Blagojevic developed the following equation:

$$r = r_o + r_e + r_p \tag{3.2a}$$

where

$$r_o = aP^n \quad \text{normal burning rate} \tag{3.2b}$$

$$r_e = \alpha G^{0.8} D^{-0.2} \exp(-\beta \rho_b r/G)$$

modified erosive burning rate of Lenoir and Robillard (3.2c)

$$r_p = (r_o^* - r_o) \exp(-G/\rho_b r\gamma)$$

plateau burning rate (3.2d)

The modification to the Lenoir and Robillard equation proposed by King [7] is

$$r = (aP^n)^2/r + \alpha G^{0.8} L^{-0.2} \exp(-\beta \rho_b r/G) \tag{3.3}$$

In this equation the normal burning rate term, aP^n, is allowed to vary with crossflow by squaring the normal burning rate and dividing the result by the total burning rate, r.

The models in this first category, especially that of Lenoir and Robillard, are the expressions most often used to predict burning rates under erosive conditions. With the exception of the constants, the equations are relatively simple to evaluate and the results generally agree with measured erosive burning data. Much experimental data is needed to evaluate the constants. The major drawback of

these models was reported by King [18]. The above equations all predict that erosive burning has a substantial dependence on the temperature of the crossflow. Marklund and Lake [22] found no such dependence, even though their data matched the Lenoir and Robillard model fairly well. The explanation for this discrepancy appears to be that good results are obtained for the Lenoir and Robillard theory only because actual data is used to select the two constants. Because of this discrepancy, the assumption that erosive burning is only the result of heat transfer from the core gas to the propellant walls must be strongly questioned.

Category 2

Models based on the alteration of transport properties in the gas phase reaction zone form the second category. Two models for composite propellants are included in this category, one by Lengelle and one by Renie and Osborn. Lengelle [8], using a modification of the Granular Diffusion Flame (GDF) Model, derives the following equation for the mass flow rate, m, under erosive conditions

$$m = C_{P_b}\left(\frac{T_f - T_s}{Q}\right)\left[\frac{\mu}{L} + \frac{8.3}{10^2}\ \frac{\rho V}{(Re_x)^{0.1}}\left(\frac{L}{\delta}\right)^n \Psi\right] \qquad (3.4a)$$

where Ψ, the blocking effect of injection, is given by

$$\Psi = \frac{\log(1+B)}{B}\left[1 + B\left(\frac{L}{\delta}\right)^{\alpha}\right]\left(\frac{1}{2+\alpha}\right) \qquad (3.4b)$$

The weaknesses of this model have been enumerated by King [1] and Kuo and Razdan [2]. Among other things, King has questioned the validity of the GDF Model. Kuo and Razdan have pointed out that the assumption of incompressible flow in the gas phase reaction zone is invalid.

The second model in this category, proposed by Renie and Osborn [9, 10], uses the Petite Ensemble Model (PEM). In this model each oxidizer particle and its surrounding binder is assumed to form a pseudopropellant with its own burning rate. The total burning rate is then calculated as a statistical summation over the oxidizer particle diameters. The mathematical expression for the total burning rate, r, is

$$r = \int_D \frac{r_d}{\alpha_d} F_d \, d(\log_e D) \qquad (3.5)$$

where, for each pseudopropellant of a given oxidizer diameter, d,

r_d = burning rate

α_d = oxidizer mass fraction

F_d = oxidizer distribution function

To solve for the total burning rate, one assumes a velocity profile and calculates transport properties. A value of

erosive burning rate may then be calculated. With this value new transport properties may be calculated, and an iterative process follows until convergence is achieved.

Renie and Osborn have suggested that the success of an erosive burning theory to provide useful information on propellant selection depends on the ability of the theory to model the combustion process accurately. For this reason they believe that their model is superior to those which are based on chemically reacting boundary layer theory. These latter models solve sets of equations for reacting turbulent boundary layers, but assume a one step reaction for the combustion process. The theory of Renie and Osborn, which does display several of the observed experimental trends listed earlier, merits further study.

Category 3

The third category, models based on chemically reacting turbulent boundary layer theory, has only one model for composite propellants. This model was proposed by Kuo and Razdan [11 - 14]. In this model the burning rate is calculated from the Arrhenius law of surface pyrolysis

$$r = A_s \exp\left\{\frac{-E_{as}}{R_u T_s}\right\} \tag{3.6}$$

The propellant surface temperature is calculated by numerically solving a set of parabolic partial differential equations derived from the conservation equations.

Kuo and Razdan state that "the most realistic analysis (of erosive burning) must consider the interaction between flame zone structure and the flow field" [11]. The present author agrees with this statement. However, the combustion in the Kuo and Razdan model is assumed to occur in a global single-step chemical reaction. Although this assumption may be over-simplified, the method proposed by Kuo and Razdan does compare well with experimental data and therefore deserves further consideration.

Category 4

Models not conforming to the basic assumptions of the first three categories include theories proposed by Parkinson, Kimov, and King. Parkinson [15, 16] and Klimov [17] both suggest that under nonerosive conditions the boundary layer is "blown off" the surface of the propellant by the transpiring gases. Both investigators claim that erosive burning begins when the turbulent boundary layer is forced onto the propellant surface by the high velocity crossflow. This suggestion does not agree with the observed results of Yamada, Goto and Ishikawa [5]. However, Yamada, Goto and Ishikawa did suggest that the laminar sublayer might be widened at the head end of the

grain by the transpiring gases. This widening of the sublayer may be related to the "blow off" phenomenon suggested by Parkinson and Klimov. On this basis the proposed model may be valid, and therefore deserves further consideration.

The last model to be considered is that of King [18 - 21]. Actually, King has proposed several modifications to his original model. The latest modification couples the idea of flame bending with turbulence effects. The flame bending phenomenon is illustrated in Fig. 2. King presents an argument to support the theory that the length of the fuel-oxidizer mixing zone is independent of crossflow. Therefore, when crossflow is present, the distance between the surface and the secondary heat release zone will be decreased. With the flame closer to the surface, the heat feedback to the propellant is increased and with it, the burning rate. The flame bending theory has been questioned by Parkinson [16] on the grounds that the displacement of the combustion zone will be large. Despite this criticism, the results of King's model compare well with experimental data. The advanced nature of this model definitely makes it one of the primary theories on erosive burning.

Of the models discussed, the Lenoir and Robillard approach produces a result which can be easily calculated and conveniently applied. The more recent models of Renie

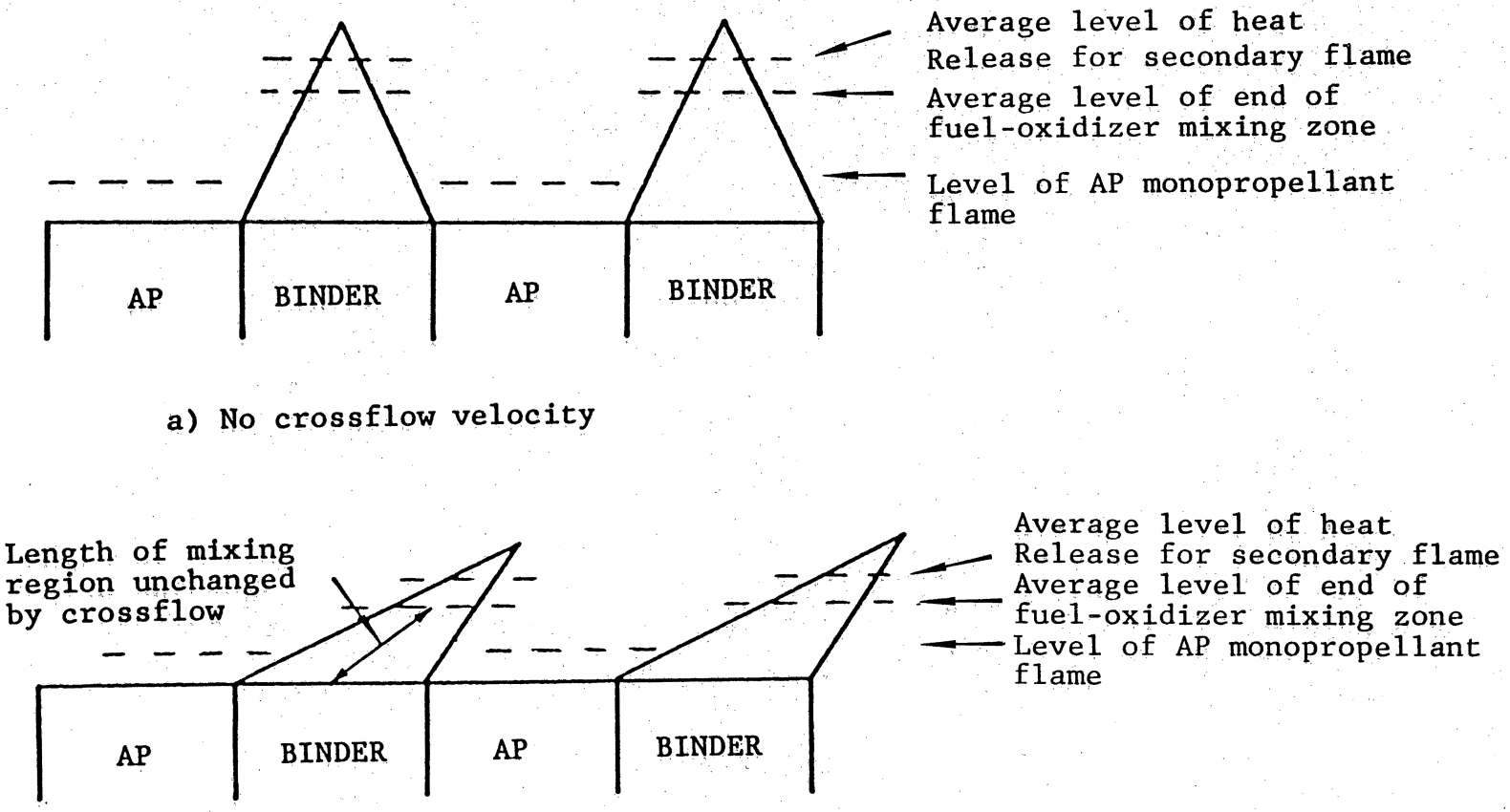

Figure 2. Schematic of Flame Bending Model [18].

and Osborn, Kuo and Razdan, Parkinson, and King incorporate expressions for effects not included in the Lenoir and Robillard model, and are generally more complex. In future experimental work, it is recommended that all of the above models be considered for comparison with data.

and Osborn, Kuo and Razdan, Parkinson, and King incorporate expressions for effects not included in the Lenoir and Robillard model, and are generally more complex. In future experimental work, it is recommended that all of the above models be considered for comparison with data.

3.2 DISCUSSION OF EXPERIMENTAL METHODS FOR MEASURING EROSIVE BURNING

In Section 2, five different experimental techniques for measuring erosive burning were reviewed: interrupted burning, x-ray flash, embedded sensors, high-speed motion pictures, and pressure-time histories. The first three methods result in only an average burning rate and therefore are not the best suited for measurement of erosive burning rates. The use of pressure-time histories is not an exact measurement, but produces a deduced burning rate from the results of a test firing. Although this method is potentially useful in design, it does not constitute an accurate experimental technique for measuring erosive burning.

The high-speed motion picture technique is the only experimental method cited in the erosive burning literature which yields instantaneous burning rates. The weakness of this method is that the measured burning rate is that of

the propellant immediately inside the window through which the camera is looking. Next to the window the flow, and therefore the burning rate, may be affected by boundary layer growth along the wall. Unwanted effects may also result if the window begins to ablate during testing.

Section 4

MICROWAVE BURNING RATE TECHNIQUE

A technique for measuring erosive burning is needed which will provide instantaneous burning rates without disrupting the internal flow or introducing edge effects. Preferably such a technique would be applicable to full scale rocket motors. The microwave technique provides these advantages. This section will describe the theory behind the microwave technique and explain its application to erosive burning.

A review of microwave burning rate methods is given by Holly [25]. All of the microwave techniques rely on the ability to detect and interpret an electromagnetic signal which has been transmitted through the propellant and reflected off of the burning surface. The incident and reflected signals add vectorially, resulting in a standing wave. However, as the propellant recedes the "standing wave" moves and increases in power. The first microwave technique relied on detecting the position of the standing wave pattern with respect to time. However, the resolution could be no better than one quarter of a wavelength. Assuming a 30GHz signal, a resolution of approximately 0.25 cm results from calculations employing the original techniques.

The ability to measure the instantaneous burning rate, and therefore transient erosive burning rates, came about when Shelton incorporated a phase meter with the microwave interferometer [26]. A phase meter is a device which continuously measures the phase angle between two microwave signals. Using a phase meter, Shelton attempted to measure the phase angle between the signal reflected off of the burning surface and a reference signal. A schematic representation of the set-up is shown in Fig. 3. The burning rate, r, may be calculated as

$$r = \left(\frac{\lambda_p}{720^\circ}\right) \frac{d\Phi_a}{dt} \tag{4.1}$$

where Φ_a is the angle between the burning surface reflection, $V_B(t)$, and a fixed reference signal, V_R. However, due to the presence of fixed reflections resulting from impedance mismatches in the transmission line, the angle measured by the phase meter is not Φ_a. The effect of fixed reflections is shown vectorially in Fig. 4, where vector V_A is the fixed reflection and vector $V_c(t)$ is the sum of the burning surface reflection, $V_B(t)$, and the fixed reflection. Because of the fixed reflection, the angle measured by the phase meter, Φ_m, is the angle between the resultant signal, $V_c(t)$, and the reference. From trigo-

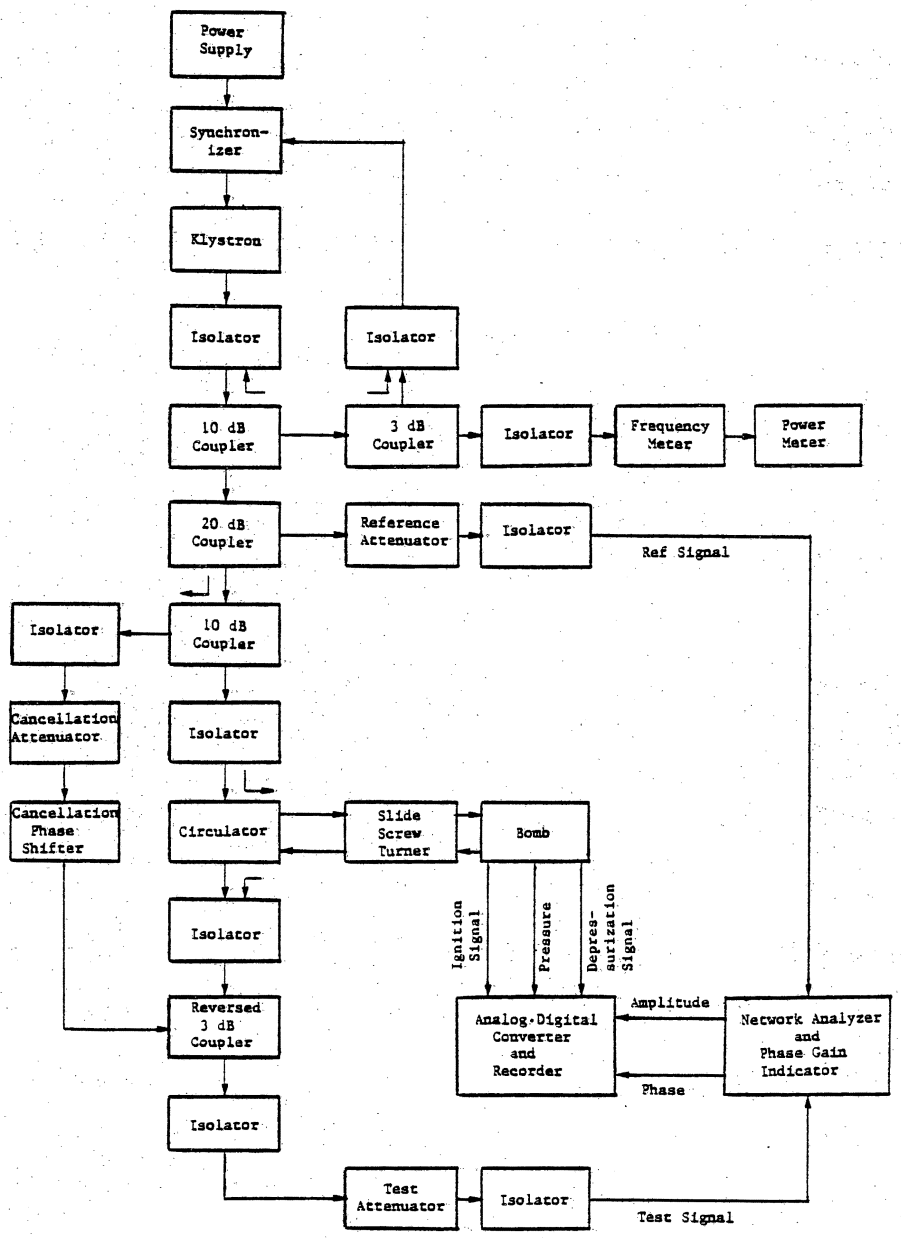

Figure 3. Schematic of Shelton Microwave Apparatus [26].

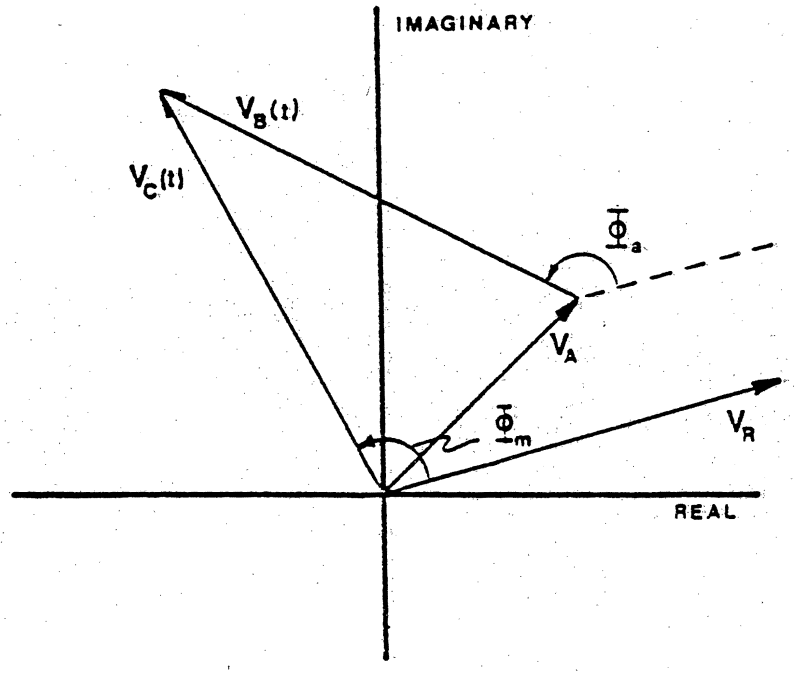

Figure 4. Vector Representation of the Reference, Fixed Reflections, and Test Signals [25].

nometry, the angles Φ_a and Φ_m are related by the following:

$$\Phi_a = \Phi_m \frac{\left(\frac{2|V_c(t)|^2}{|V_B(t)|^2}\right)}{\left(\frac{|V_C(t)|^2}{|V_B(t)|^2} - \frac{|V_A|^2}{|V_B(t)|^2} + 1\right)} \tag{4.2}$$

Therefore, solving for the burning rate involves determining certain angles and magnitudes from continuous relative phase and amplitude data.

A schematic diagram of the microwave apparatus at VPI&SU is shown in Fig. 5. The heart of the system is the Hewlett Packard model 8410B Network Analyzer. This device measures both relative phase and relative amplitude of the microwave signal. With the continuous data provided by the network analyzer, the parameters in the equations developed by Shelton may be calcuated. A method for determining these parameters was developed by Holly [25] at VPI&SU. Starting with a simplified representation of a slab burner, as shown in Fig. 6, Holly modeled the situation as a time-dependent burning surface reflection and one fixed reflection. The modeled system and the corresponding vector diagram are shown in Figs. 7 and 8, respectively. Note that the vector, V_A, is the sum of the fixed reflections, V_1, V_2, and V_3.

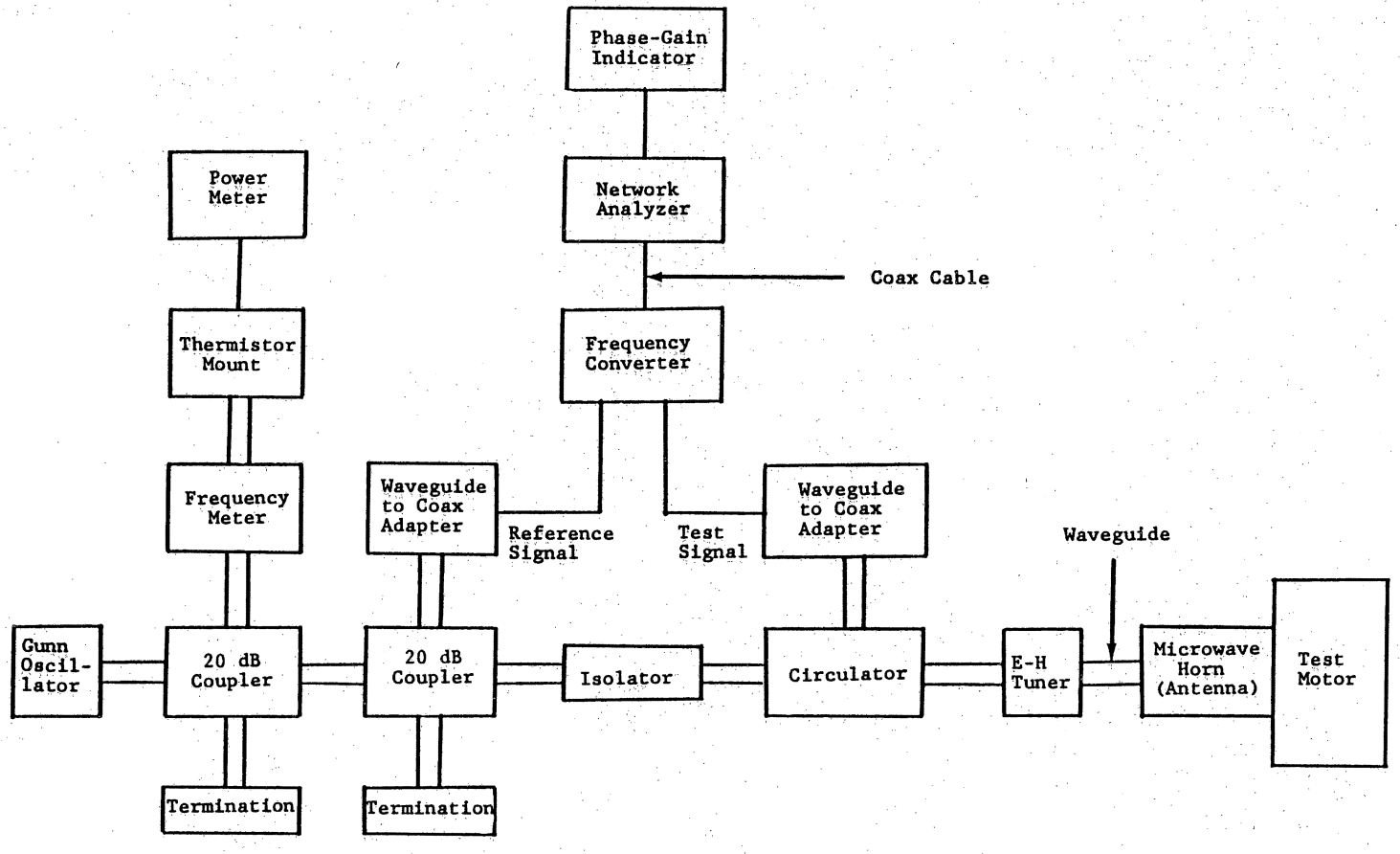

Figure 5. Schematic of VPI&SU Microwave Apparatus.

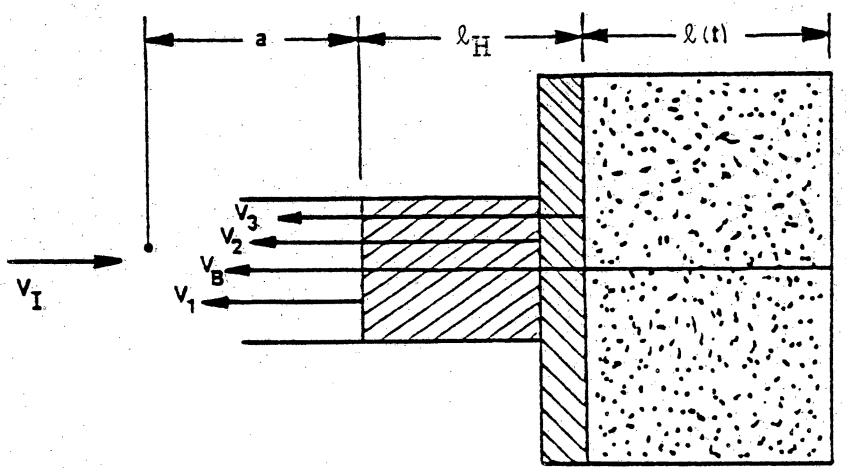

Figure 6. Model of Slab Burner [25].

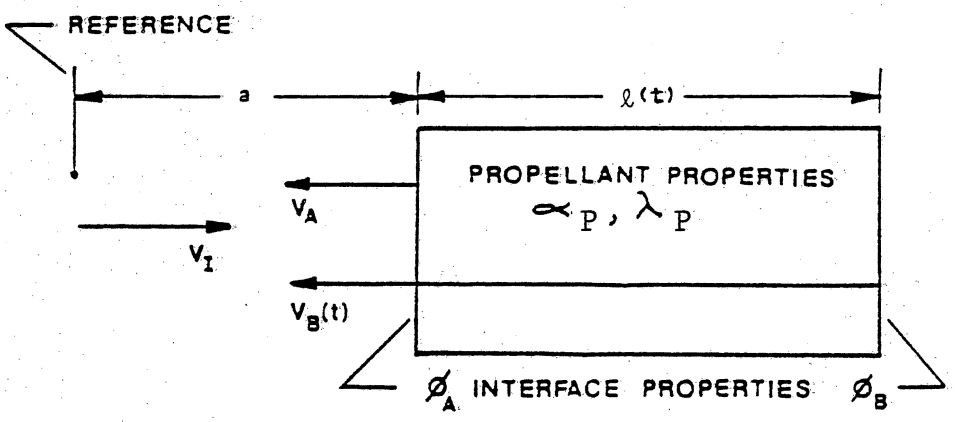

Figure 7. Modeled System [25].

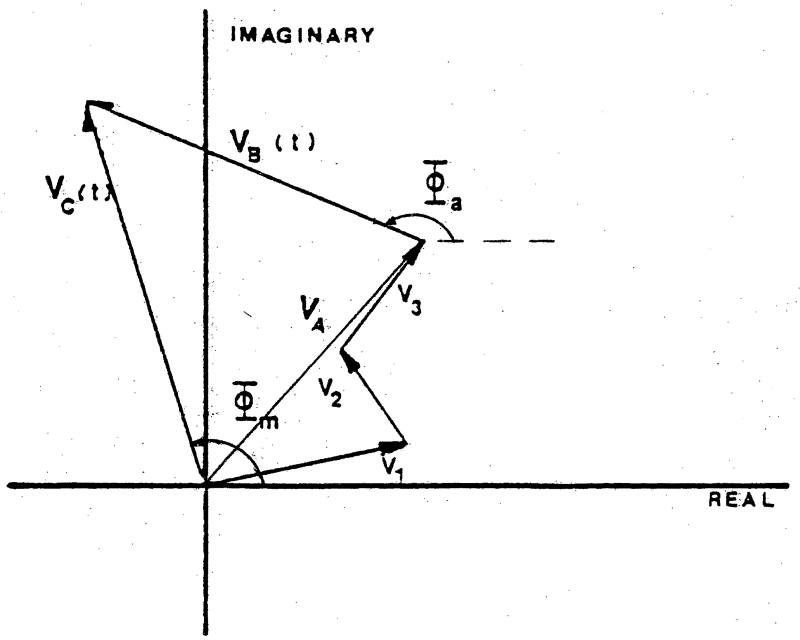

Figure 8. Vector Representation of Modeled System [25].

A signal incident on an interface is shown schematically in Fig. 9. In his model, Holly assumed that the signals strike all interfaces perpendicularly, resulting in perpendicular reflections. Each interface has a reflection coefficient, Γ, and a transmission coefficient, T. When a signal is reflected from an interface, it undergoes a phase jump, $\emptyset$. The transmission coefficient, reflection coefficient, and phase jump are all functions of the impedance mismatch and the source frequency. From the theory of electromagnetic propagation, the signals V_A and $V_B(t)$ may be mathematically described as follows:

$$V_A = E_o \Gamma_A \exp\{j(2k_w a_w + \emptyset_A)\} \tag{4.3}$$

$$V_B(t) = E_o T_A T_A' \exp\{-2(\alpha_H \ell_H + \alpha_p \ell(t))\} \cdot \exp\{j(2k_w a_w + 2k_p \ell(t) + \emptyset_B)\} \tag{4.4}$$

where T_A' = Transmission coefficient for propagation in the direction opposite the incident signal.

Figure 10 shows the vector diagram incorporating the phase angles described in the above equations. Combining the path length phase shift, $k_w a$, together with the interface phase jumps, $\emptyset_A$ and $\emptyset_B$, the reflection phase shifts, $\emptyset_A'$ and $\emptyset_B'$, result. A vector diagram describing these parameters is shown in Fig. 11. Assuming the transmission and

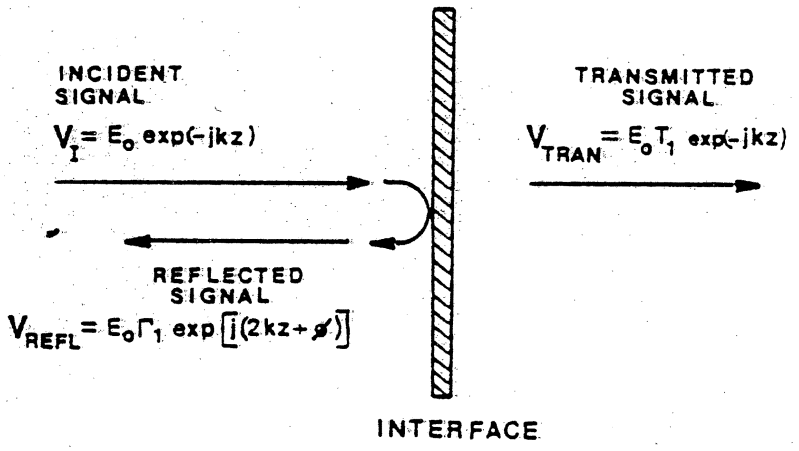

Figure 9. Microwave Signal Incident on an Interface [25].

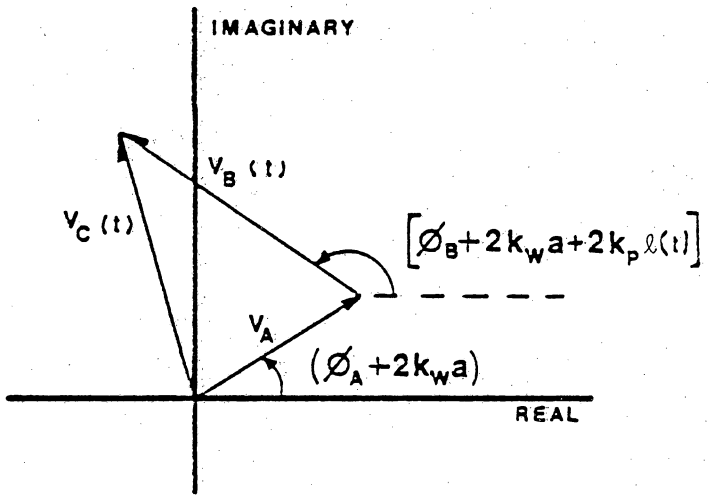

Figure 10. Vector Representation of Modeled System with Specified Phase Angles [25].

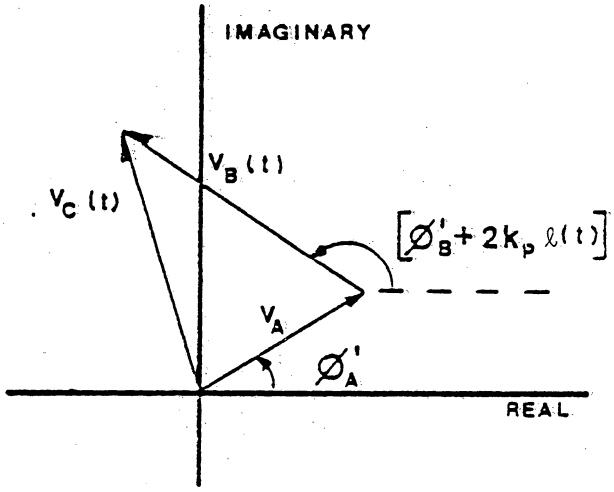

Figure 11. Vector Representation of Modeled System with Lumped Parapmeters [25].

reflection coefficients, as well as the incident signal and horn attenuation, to be constant, the equations reduce to

$$V_A = |V_A|_{cf} \exp\{j\phi_A'\} \tag{4.5}$$

$$V_B(t) = |V_A|_{cf} \exp\{-2\alpha_p \ell(t)\} \exp\{j(\phi_B' + 2k_p \ell(t))\} \tag{4.6}$$

The magnitudes of these vectors may be written as

$$|V_A| = |V_A|_{cf} \tag{4.7}$$

$$|V_B(t)| = |V_B|_{cf} \exp\{-2\alpha_p \ell(t)\} \tag{4.8}$$

In terms of vector magnitudes and lumped parameters, the measured phase angle, Φ_m, is given by

$$\Phi_m(t) = \tan^{-1}\left[\frac{|V_B(t)| \sin(\phi_B' + 2k_p \ell(t)) + |V_A| \sin(\phi_A')}{|V_B(t)| \cos(\phi_B' + 2k_p \ell(t)) + |V_A| \cos(\phi_A')}\right] \tag{4.9}$$

The relative amplitude output of the network analyzer may be expressed as [27]:

$$\text{Amp}(t) = \text{GAIN} - \text{XNULL} + 20 \log_{10}\left[\frac{|V_c(t)|}{|V_R|}\right] \tag{4.10}$$

where GAIN = dial setting of the gain control on the network analyzer

XNULL = test channel gain which if internally imposed by the network analyzer would make the output from the relative gain indicator equal to zero volts.

V_R = magnitude of reference signal

The parameter GAIN is set by the operator. Russell [27] has developed a method for determining XNULL. The magnitude of the reference signal may be measured before each test and is assumed to be constant during the test. Therefore, equation 4.10 may be solved explicitly for $|V_c(t)|$:

$$|V_c(t)| = |V_R| \log_{10}^{-1}\left[\frac{\text{Amp}(t) + \text{XNULL} - \text{GAIN}}{20}\right] \qquad (4.11)$$

The magnitude of the resultant signal may be related to the unknown parameters as follows:

$$|V_c(t)| = \left[|V_B(t)|^2 + |V_A|^2 + 2|V_B(t)|\,|V_A| \cos(\phi_A' - 2k_p\ell(t) - \phi_B')\right]^{\frac{1}{2}} \qquad (4.12)$$

For determination of the propellant burning rate, the problem is now one of solving for the seven unknowns, k_p, α_p, $|V_B|_{cf}$, $|V_A|$, ϕ_A', ϕ_B', and $\ell(t)$. The propellant parameters, k_p and α_p, may be found experimentally [25]. Since the initial length of the propellant is known and the final

length is zero, equations 4.9 and 4.12 may be written for the time of ignition and the time of burnout. Values for $|V_c(0)|, |V_c(t_f)|, \Phi_m(0), \Phi_m(t_f)$ come directly from instantaneous phase and amplitude data and the use of equation 4.11. The four equations are:

$$|V_c(0)| = \sqrt{|V_B|_i^2 + |V_A|^2 + 2|V_B|_i|V_A| \cos(\phi_A' - 2k_pL_p - \phi_B')} \quad (4.13)$$

$$\Phi_m(0) = \tan^{-1}\left[\frac{|V_B|_i \sin(\phi_B' + 2k_pL_p) + |V_A| \sin(\phi_A')}{|V_B|_i \cos(\phi_B + 2k_pL_p) + |V_A| \cos(\phi_A')}\right] \quad (4.14)$$

$$|V_c(t_f)| = \sqrt{|V_B|_{cf}^2 + |V_A|^2 + 2|V_B|_{cf}|V_A| \cos(\phi_A' - \phi_B')} \quad (4.15)$$

$$\Phi_m(t_f) = \tan^{-1}\left[\frac{|V_B|_{cf} \sin(\phi_B') + |V_A| \sin(\phi_A')}{|V_B|_{cf} \cos(\phi_B) + |V_A| \cos(\phi_A')}\right] \quad (4.16)$$

where

$$|V_B|_i = |V_B|_{cf} \exp(-2\alpha_pL_p) \quad (4.17)$$

Holly developed a program to solve these four equations making use of a subroutine from the International Mathematical Society Library (IMSL). Once the parameters $|V_B|_{cf}$ and $|V_A|$ are known, Shelton's equations, 4.1 and 4.2, may be solved for the burning rate. Holly also

proposed his own method for finding the burning rate. His technique requires that equations 4.9 and 4.12 be solved simultaneously for the instantaneous length, $\ell(t)$. The burning rate is then calculated as the change in length divided by the elapsed time between data points. Both methods provide an accurate value of burning rate for each relative phase and amplitude data point.

A data acquisition system for use with this research has been assembled at VPI&SU. The system consists of a TRS 80 Model III microcomputer, an analog to digital converter, a printer, and a modem for access to the mainframe. A block diagram of the system is shown in Fig. 12. Four data channels will be recorded: relative phase, relative amplitude, and two pressure signals. Using a 1 kHz sampling rate with this data acquistion system, the present capacity of the computer will permit continuous measurement of the transient phenomenon of erosive burning over a period of approximately four seconds.

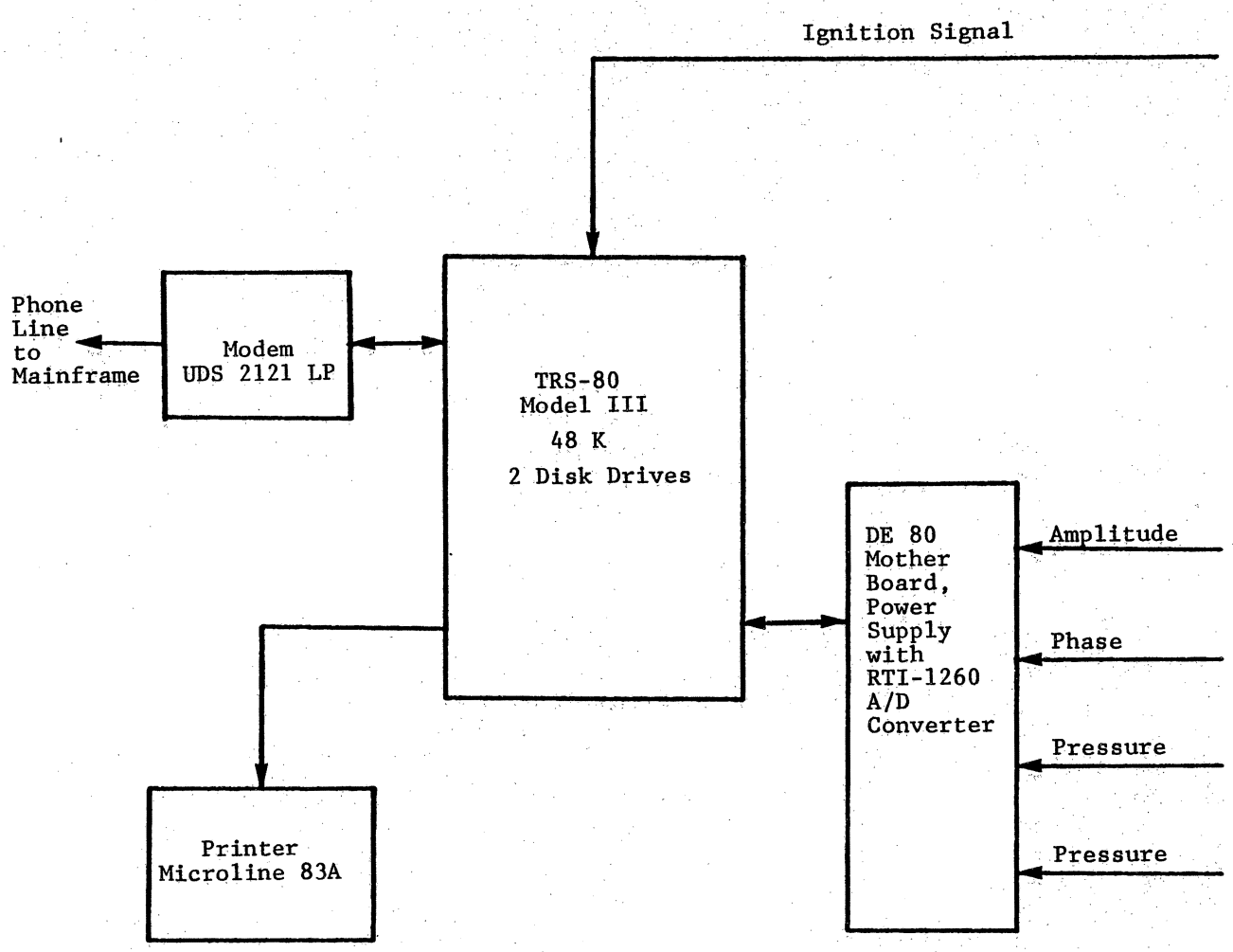

Figure 12. Schematic of Data Acquisition System.

Section 5

DESIGN OF A PROPOSED MICROWAVE EROSIVE BURNING TESTER

As discussed in Section 2.2, several devices have been used to measure erosive burning. Section 4 explained the microwave burning rate measurement technique and the advantages of using it to measure erosive burning. This section will propose a design for an erosive burning tester utilizing microwaves. All calculations are presented in Appendix A.

Considerations in the design of an erosive burning tester require:

1. The ability to have crossflow velocities ranging from Mach 0.2 to Mach 1.
2. A test section long enough to simulate the hydrodynamics found in real rocket motors.
3. The ability to measure the burning rate away from the walls of the test section.
4. Enough clearance over the propellant to prevent the boundary layer growing along the chamber surface from interfering with the combustion process.
5. The minimum mass flow and thrust necessary to fulfill the above requirements.

It appears that a practical erosive burning tester has two sections: a gas generator and a test section. A schematic of an erosive burning tester is shown in Fig. 13. The gas generator provides the high velocity gases needed to induce erosive burning, while the test section provides for the simulation of the aerodynamics of an actual rocket motor. The exhaust gases from the gas generator pass over the propellant in the test section, thus creating high crossflow velocities. The design study that follows will utilize a test section with a 30.5 cm long slab of propellant. The flow conditions within the test section are such that the flow field over the propellant may be approximately modeled as flow over a flat plate with injection. As the gases accelerate through the test section the flow field will simulate that of an actual rocket motor. A two-dimensional nozzle with no diverging section would be used for the tests with crossflow velocities under Mach 1. However, the following analysis will assume a sonic crossflow velocity, corresponding to a nozzleless test. The assumed propellant properties and design parameters are presented in Appendix A. At this time, a propellant web thickness of 2.5 cm will be assumed. After the early experiments with the erosive burning tester have been analyzed, a minimum acceptable value of web

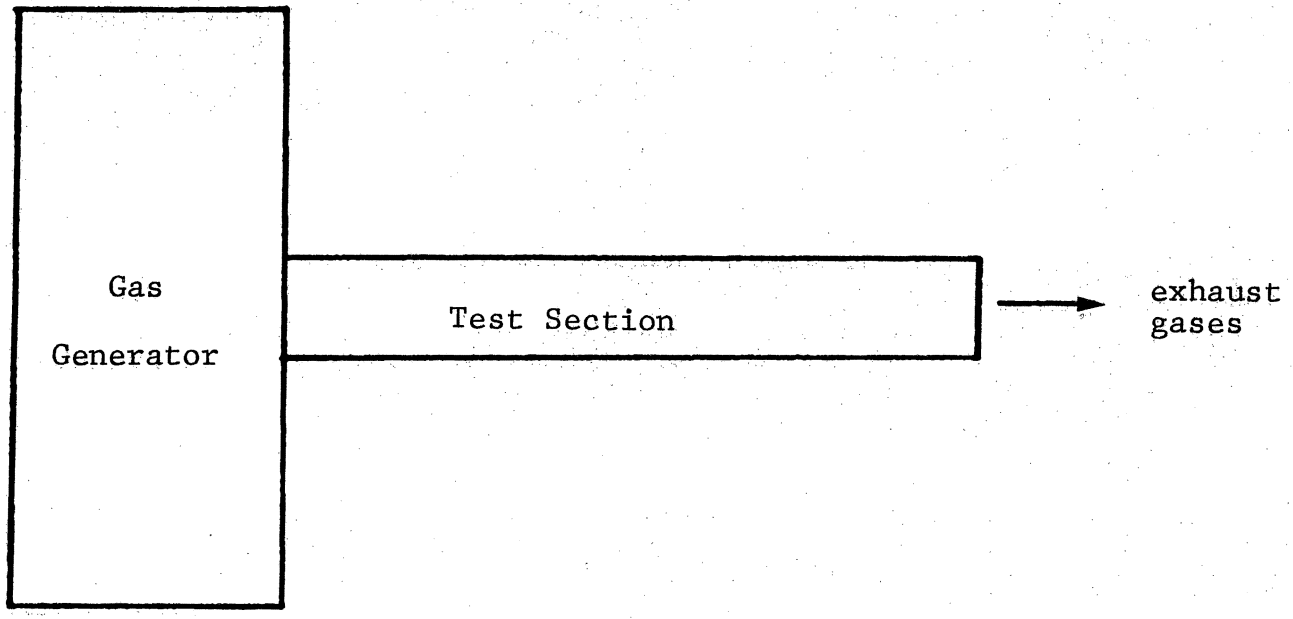

Figure 13. Schematic of Erosive Burning Tester.

thickness which yields repeatable reliable results will be selected.

The first step in the design of an erosive burning tester is to determine the necessary crossflow velocity. The velocity as a function of Mach number is given by

$$V = M\sqrt{\frac{kR_u T}{MW}} \tag{5.1}$$

The required velocity for sonic flow with the assumed propellant properties is 1,035 m/s (See Appendix A). The velocity resulting from combustion of propellant in the test section may be calculated from the continuity equation,

$$\dot{m} = \rho_b A_b r = \rho_p V_p A \quad , \tag{5.2a}$$

giving the result

$$V_p = \frac{\rho_b L}{\rho_p h} r \tag{5.2b}$$

where L = length of propellant upstream of the burning rate measurement

h = initial height of crossflow area over the propellant in the test section.

Assuming values of 25.4 cm and 1.9 cm for L and h, respectively, the test section provides only 44.7 m/s, or

4% of the required velocity. Therefore the gas generator must supply most of the mass flow to produce the crossflow velocity.

The total mass flow of the tester may be calculated from the equation

$$m = \rho A(V_D + V_P) \tag{5.3}$$

assuming that the densities of the driver exhaust gases and the propellant gases are equal. For the assumed propellant with sonic velocity, the resulting mass flow is given by

$$m = 0.447A \quad (kg/s) \tag{5.4}$$

where the crossflow area, A, is in square centimeters. The crossflow area must be large enough to prevent the boundary layer growth on the three chamber walls from interfering with the flow in the area of the burning rate measurement. A large mass flow rate would allow for a large crossflow area. However, a high mass flow rate requires a large total mass of propellant from the gas generator. For economy and safety reasons, the maximum mass flow rate was chosen to be 4.3 kg/s. Using this value and equation 5.4, the area over the propellant would be initially 9.62 cm^2.

As previously mentioned, the dimensions of this rectangular area must be selected so as to prevent the boundary layer growth from interferring with the combustion process. This task is accomplished by calculating the thickness of the boundary layer on the chamber walls and allowing for the blocking effect of injection. The momentum thickness and boundary layer thickness may be calculated from the following equations [28]:

$$\delta_2 = \frac{0.036\nu^{0.2}}{u_\infty^{3.29}} \left[u_\infty^{3.86} x \right]^{0.8} \tag{5.5}$$

$$\frac{\delta}{\delta_2} = 10.31 \tag{5.6}$$

These equations assume a constant free stream velocity. Although the velocity in the test section is changing, the pressure gradient is favorable from a boundary layer viewpoint. Therefore, these equations are assumed to yield larger values than will actually exist. The boundary layer will be largest during the tests with lower velocities. Assuming a Mach number of 0.2 and using the data given in the Appendix, the momentum thickness and boundary layer thickness are 0.07 cm and 0.74 cm, respectively. It was assumed that the flow height should be a minimum of twice the boundary layer thickness. Therefore, to avoid the blocking effect of the boundary layer and to minimize the

total mass flow, the optimum geometry was chosen to be a height of 1.9 cm and therefore a width of 5.06 cm, as shown in Fig. 14. This geometry prevents the boundary layer growth along the bottom of the upper surface of the test section from interfering with the combustion process.

As the propellant recedes, the flow area will increase, resulting in a lower crossflow velocity. At any time the velocity may be calculated from the continuity equation:

$$V = \frac{m}{\rho A} \tag{5.7}$$

Assuming a constant mass flow of 4.3 kg/s and using equation 5.5, the velocity at burnout will be 287 m/s, or Mach 0.28. The thrust generated by the tester is given by

$$F_e = V_e m + (P_e - P_3)A_e \tag{5.8}$$

For the given assumptions and flow area the thrust would never exceed 15.7 kN.

As a final calculation for the test section, an estimate of the burning rate augmentation ratio, r/r_o, will be determined using the Lenoir and Robillard model, equation 3.1a. The constants, α and β, will be assumed from the original work of Lenoir and Robillard [3]. Once

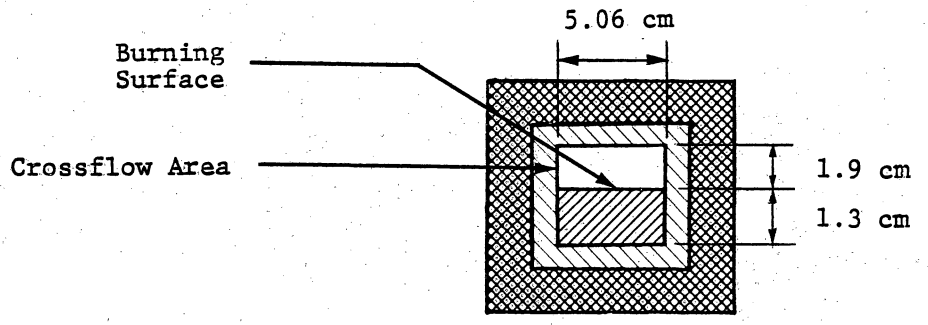

a) End View

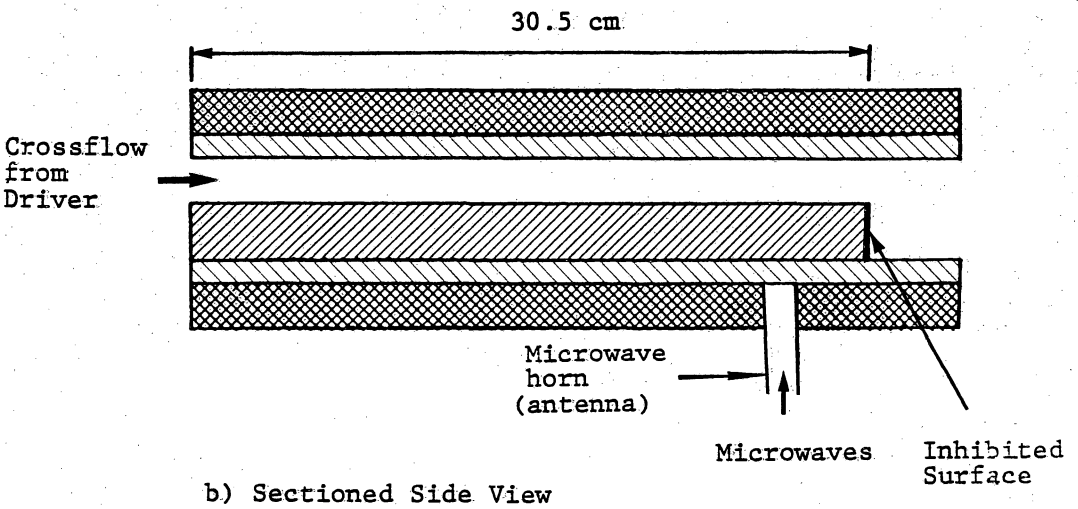

b) Sectioned Side View

Steel Chamber

Propellant

Phenolic Insulation

Figure 14. Test Section of Erosive Burning Tester.

the tester is operational, the constants would have to be evaluated from actual data for each propellant. Using the assumed constants and the static properties for M = 1, equation 3.1a becomes:

$$r = 0.709 + 1.66 \exp \{ -0.204\ r \} \qquad (5.9a)$$

and

$$r = 1.85 \quad \text{cm/s} \qquad (5.9b)$$

Therefore

$$r/r_o = 2.6 \qquad (5.9c)$$

Similarly, the augmentation ratio is 1.55 at burnout for the proposed design.

Since some investigators suggest that erosive burning is not affected by the temperature or composition of the crossflow [22], the gas generator for the erosive burning tester could be fueled by either a liquid or a solid propellant. It a solid propellant with a density of 0.172 g/cm^3 and a burning rate of 0.84 cm/s were used, a surface area of 0.298 m^2 would be required to produce the necessary mass flow. One possible grain configuration for this

surface area would be a cylindrical grain with a single perforation. For example, a grain with a 25.4 cm diameter perforation would have to be 37.3 cm in length. A star grain grain configuration or a similar geometry could accomplish the same result with a slightly shorter grain.

If a liquid fuel is to be used, a monopropellant would be preferred because there would no mo mixing problems. Two possible monopropellants are hydrazine and ethylene oxide. Ignition of the fuel would be achieved using a solid propellant igniter. Decomposition is sustained by a thermal catalyst bed composed of stainless steel or a platinum catalyst. An example of a gas generator using hydrazine as fuel is shown in Fig. 15. In this instance, stainless steel is assumed to be used as the thermal catalyst bed. Once the bed is heated by the igniter, the hydrazine decomposition would be sustained by the catalyst bed.

Of the two types of fuels under consideration, a solid propellant is the more predictable from a safety standpoint. Also, there already exists a magazine for storing some of the gas generator grains. The advantage of the liquid propellant is that the mass flow could be regulated and controlled to some extent. However, the Rocket Test Facility at VPI&SU would have to be modified to handle

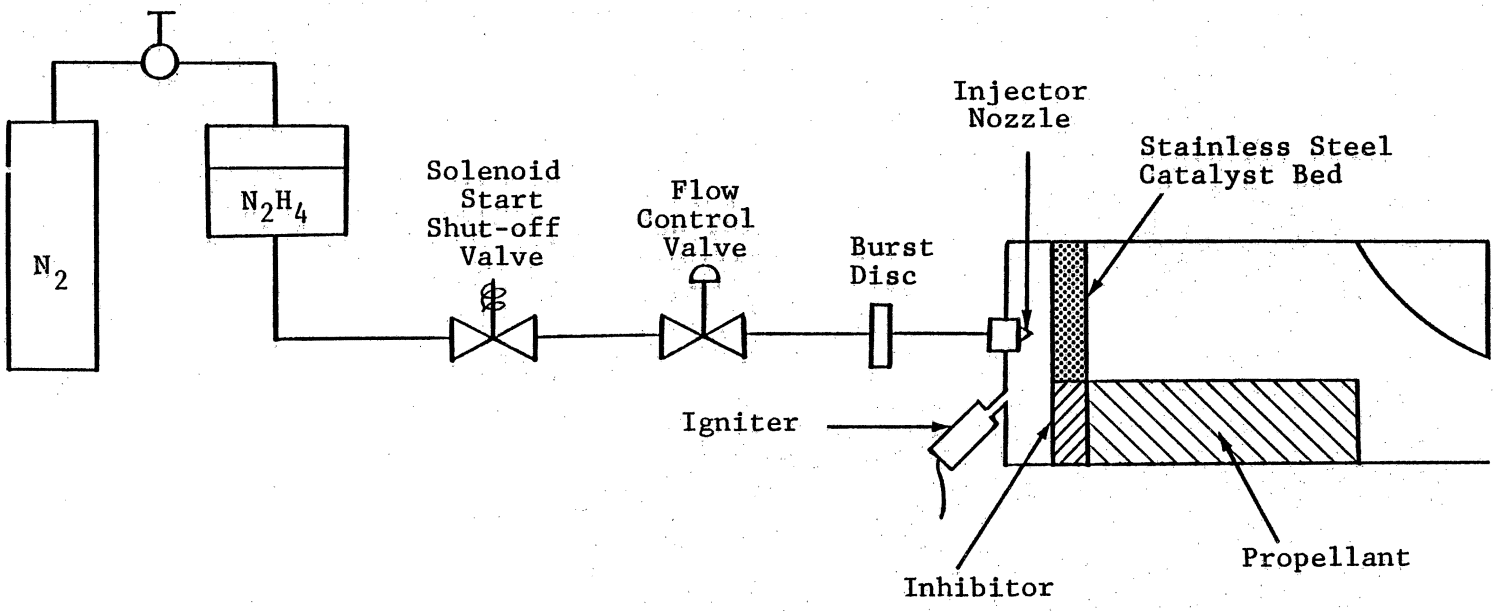

Figure 15. Erosive Burning Tester with Gas Generator Fueled by Hydrazine.

liquid propellants. At this time no decision has been made as to which type of propellant will be used in the gas generator.

Section 6

PRELIMINARY TESTING

Before finalizing the design of the proposed erosive burning tester, a slab burner will be used to verify the microwave measuring technique and the data reduction software. To accomplish this task a slab burner has been constructed by the sponsor of this research, the Naval Ordnance Station. Facilities for test firing the gas generator have already been completed at VPI&SU. This section will describe the gas generator and the facilities.

The gas generator, shown in Figs. 16, 17, and 18, is constructed of 1.27 cm (1/2 inch nominal) steel plate welded together. The bottom is 1.91 cm (3/4 inch nominal) steel plate. The overall dimensions are 42.7 x 19.4 x 12.2 cm. The propellant will be cast in a phenolic box which fits securely inside the steel chamber. The propellant slab burns on the top surface only. The burning surface has an area of 30.5 cm^2. The nozzle is located on one end of the chamber. The microwave horn will fit inside either of the tubes located on the bottom of the chamber. The microwaves will exit the horn, pass through the bottom of the phenolic box, and proceed through the propellant. After reflecting off the burning surface the microwaves

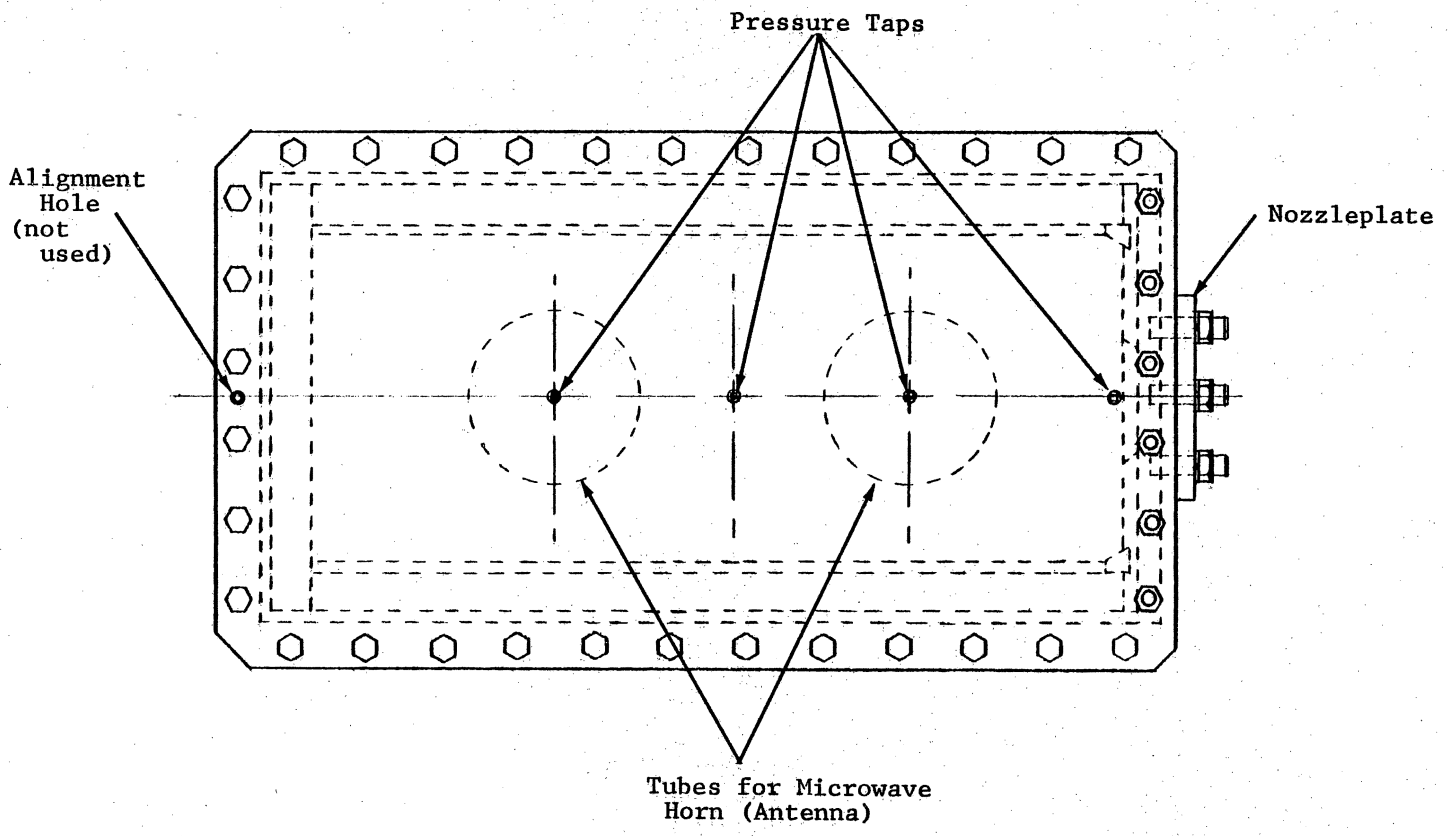

Figure 16. Gas Generator: Top View.

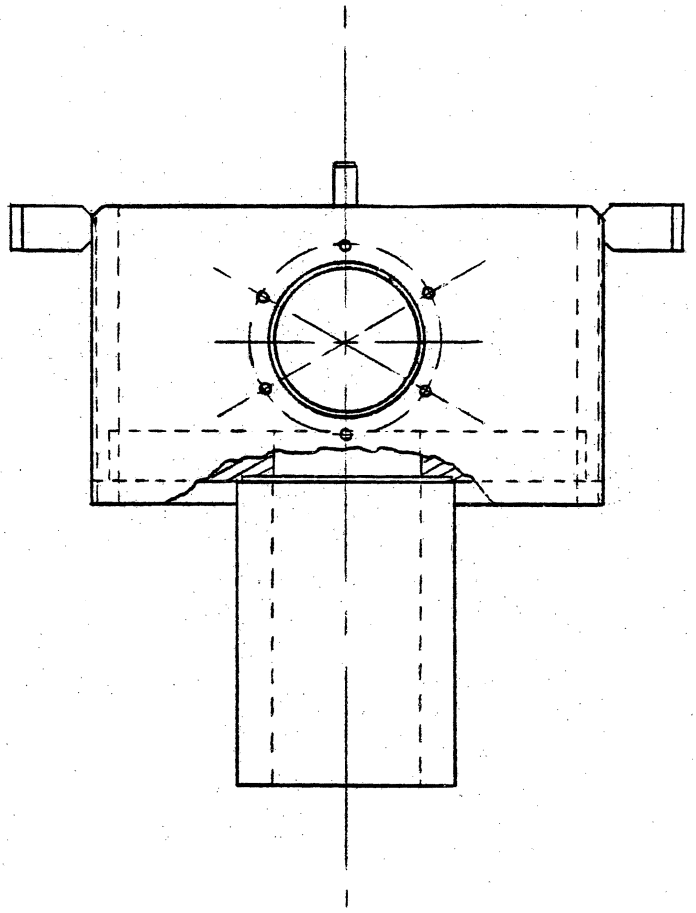

Figure 17. Gas Generator: End View.

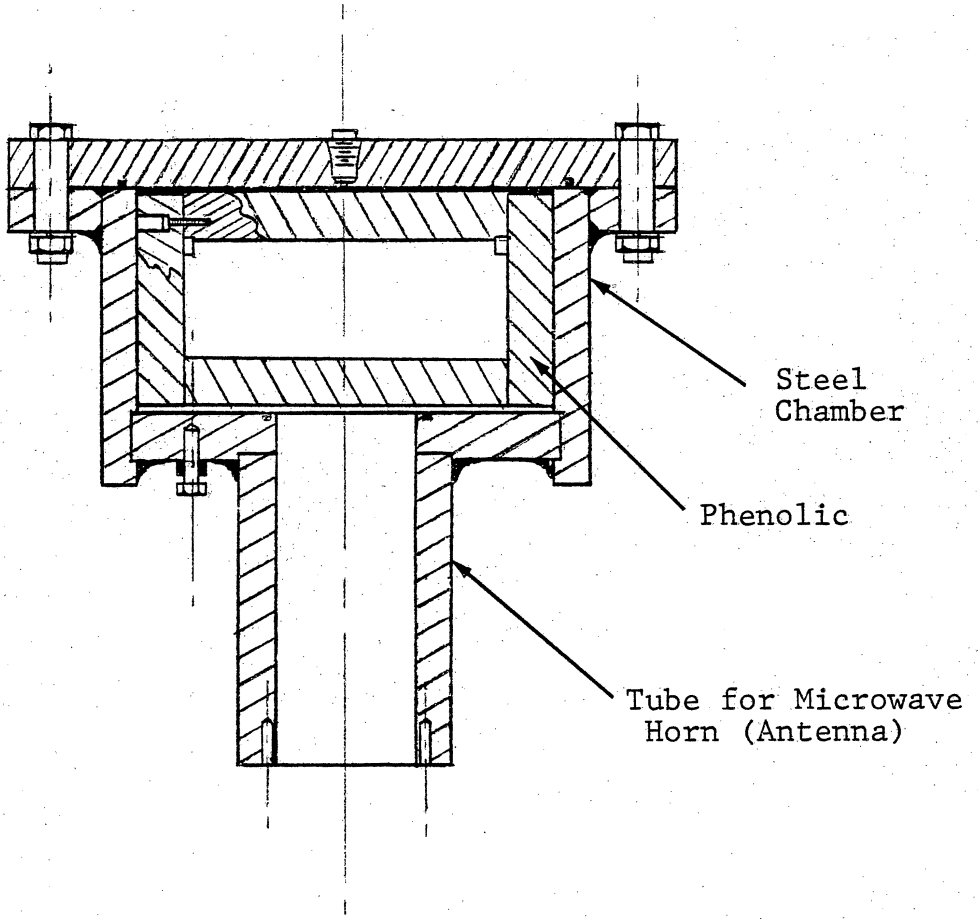

Figure 18. Gas Generator: Sectioned View.

will return through the propellant and the phenolic box and into the horn.

At this writing, two test firings have been performed at the Naval Ordnance Station. Although the tests were deemed successful, problems with nozzle erosion and non-neutrality of the pressure-time history are being investigated. Once the gas generator is delivered to the test facility at VPI&SU, initial tests on the microwave system will be performed. After the data have been reduced and analyzed, a test plan will be devised. Twenty test firings are tentatively planned. With the information gathered from these tests, the design of the erosive burning tester can be finalized.

The test facilities consist of two buildings located 6 km west of the VPI&SU campus at Price's Fork Research Center. A floor plan of the buildings is given in Fig. 19. The test cell is constructed of concrete blocks filled with sand. The roof is of wooden construction and is fastened so as to blow off in the event of an explosion. The door of the test cell rolls upward to provide a large opening for the exhaust gases of the gas generator. The instrumentation room is a prefabricated fiberglass building built on a metal skid. It is equipped with a telephone, electricity, heating, and air conditioning. The wall separating the two buildings is made of double reinforced concrete.

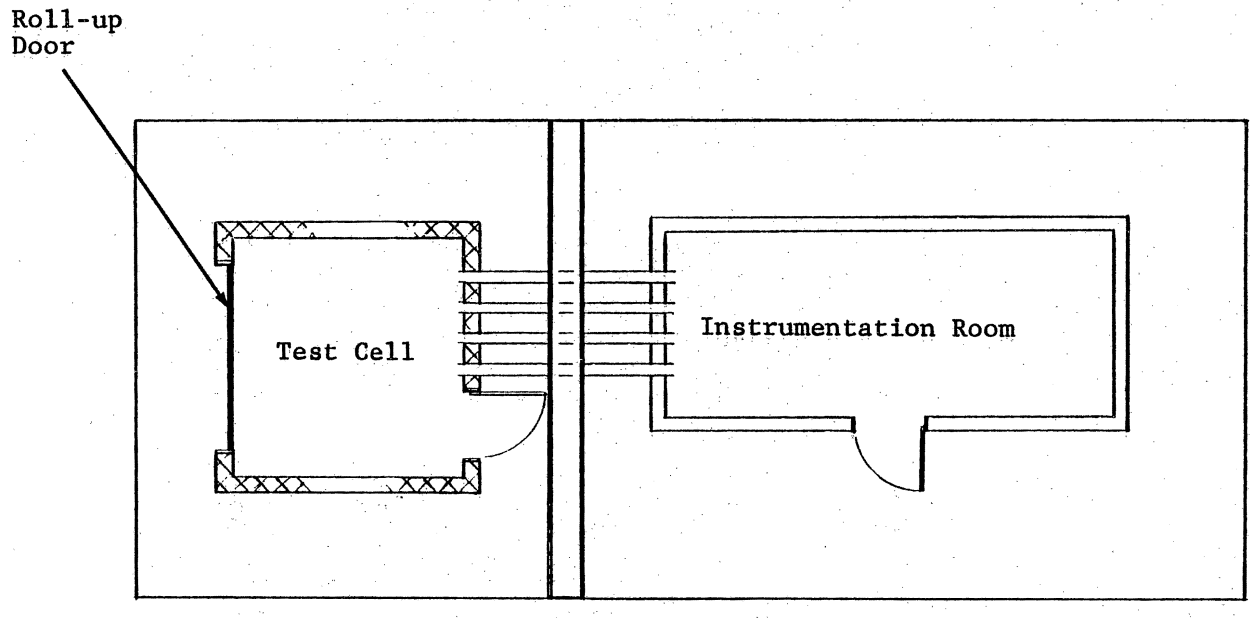

Figure 19. Rocket Test Facility Floor Plan.

The connecting tubes, made of 10 cm PVC conduit, provide a means of running the instrumentation wires and waveguide between the buildings.

Section 7

CONCLUSIONS

A review of present theories to predict erosive burning in composite propellants has been presented. From available data, the theories of Renie and Osborn, Kuo and Razdan, Parkinson, and King were considered to be the most advanced while that of Lenoir and Robillard was considered to be the most easily applied in practice. Methods for the measurement of erosive burning in test appratus were discussed. A detailed development of the theory for the microwave technique was presented.

Assuming the use of the microwave technique, a preliminary design for an erosive burning tester was developed. By utilizing microwave interferometry, this apparatus could be used to measure the burning rate under crossflow velocities between Mach 0.2 and 1.0.

After final testing of the microwave measuring technique, the erosive burning tester should be built and used to evaluate the present erosive burning theories.

Section 8

BIBLIOGRAPHY

1. King, M. K., "A Model of the Erosive Burning of Composite Propellants," AIAA Paper No. 77-930, July 1977.

2. Kuo, K. K., and Razdan, M. K., "Review of Erosive Burning of Solid Propellants," 12th JANNAF Combustion Meeting, CPIA Publication 273, Vol. II, 1975, pp. 323-338.

3. Lenoir, J. M., and Robillard, G., "A Mathematical Method to Predict the Effects of Erosive Burning in Solid-Propellant Rockets," Sixth Symposium (International) on Combustion, 1957, pp. 663-667.

4. Lawrence, W. J., Matthews, D. R., and Deverall, L. I., "The Experimental and Theoretical Comparison of the Erosive Burning Characteristics of Composite Propellants," AIAA Paper No. 68-531, June 1968.

5. Yamada, K., Goto, M., and Ishikawa, N., "A Simulative Study of the Erosive Burning of Solid Rocket Motors," AIAA Paper No. 75-1201, October 1975.

6. Jojic, B., and Blagojevic, DJ., "Theoretical Prediction of Erosive Burning Characteristics of Solid Rocket Propellant Based on Burning Rate Dependence of Pressure and Initial Temperature and Its Energetic Characteristics," AIAA Paper No. 76-697, July 1976.

7. King, M. K., "A Modification of the Composite Propellant Erosive Burning Model of Lenoir and Robillard," Combustion and Flame, Vol. 24, 1975, pp. 365-368.

8. Lengelle, G., "Model Describing the Erosive Combustion and Velocity Response of Composite Propellants," AIAA Journal, Vol. 13, No. 3, March 1975, pp. 315-322.

9. Renie, J. P., and Osborn, J. R., "Erosive Burning," AIAA Paper No. 79-0165, January 1979.

10. Renie, J. P., and Osborn, J. R., "Pressure and Velocity Coupled Response of Composite Solid Propellants Based Upon a Small Perturbation Analysis," AIAA Paper No. 81-1556, July 1981.

11. Razdan, M. K., Erosive Burning Study of Composite Solid Propellants by the Reacting Turbulent Boundary-Layer Approach, Ph.D. Dissertation, Department of Mechanical Engineering, Pennsylvania State University, March 1979.

12. Razdan, M. K., and Kuo, K. K., "Erosive Burning Study of Composite Solid Propellants by Turbulent Boundary-Layer Approach," AIAA Journal, Vol 17, No. 11, November 1979, pp. 1225-1233.

13. Razdan, M. K., and Kuo, K. K., "Measurements and Model Validation for Composite Propellants Burning Under Cross Flow of Gases," AIAA Journal, Vol 18, No. 6, June 1980, pp. 669-677.

14. Razdan, M. K., and Kuo, K. K., "Turbulent Flow Analysis of Erosive Burning of Cylindrical Composite Solid Propellants," AIAA Journal, Vol. 20, No. 1, January 1982, pp. 122-128.

15. Parkinson, R. C., and Penny, P. D., "A Transpired Boundary Layer Model of Erosive Burning," AIAA Paper No. 78-980, July 1978.

16. Parkinson, R. C., "Erosive Burning as a Boundary Layer Phenomenon in Rocket Motors," AIAA Paper No. 80-1208, July 1980.

17. Klimov, A. M., "Erosive Burning of Propellants," Combustion, Explosion and Shock Waves, USSR, Vol. 11, No. 5, 1975, pp. 678-681.

18. King, M. K., "Erosive Burning of Composite Propellants," 13th JANNAF Combustion Meeting, CPIA Publication 281, Vol. II, September 1976, pp. 407-435.

19. King, M. K., "Model for Steady State Combustion of Unimodal Composite Solid Propellants," AIAA Paper No. 78-216, January 1978.

20. King, M. K., "Erosive Burning of Composite Solid Propellants: Experimental and Modeling Studies," AIAA Paper No. 78-979, July 1978.

21. King, M. K., "A Model of the Effects of Pressure and Crossflow Velocity on Composite Propellant Burning Rate," AIAA Paper No. 79-1171, June 1979.

22. Marklund, T., and Lake, A., "Experimental Investigation of Propellant Erosion," ARS Journal, Vol. 3, No. 2, February 1960, pp. 173-178.

23. Peretz, A., "Experimental Investigation of the Erosive Burning of Solid-Propellant Grains with Variable Port Area," AIAA Journal, Vol 6., No. 5, May 1968, pp. 910-912.

24. Sturm, E. J., and Reichenbach, R. E., "An Experimental Investigation of Solid-Propellant Erosive Burning in an Acceleration Field," AIAA Journal, Vol. 9, No. 10, October 1971, pp. 1941-1944.

25. Holly, H. M., An Analysis of Solid Propellant Burn Rate Information Obtained from a Microwave Doppler Phase Shift Interferometer, M.S. Thesis, Department of Mechanical Engineering, Virginia Polytechnic Institute and State University, November 1981.

26. Shelton, S. V., "A Technique for Measurement of Solid Propellant Burning Rates During Rapid Pressure Transients," Bulletin of the 4th ICRPG Combustion Conference, CPIA Publication 162, Vol. I, December 1967, pp. 361-372.

27. Russell, L. H., Burning Velocities of a Solid Propellant, via a Microwave Technique, at Elevated Pressures and Pressurization Rates, Ph.D. Dissertation, University of Pittsburgh, 1979.

28. Kays, W. M., and Crawford, M. E., Convective Heat and Mass Transfer, McGraw-Hill, 1980.

APPENDIX A

Typical propellant properties and assumed design parameters:

Calculated for typical product gases at M = 1.0	Specific heat ratio:	$k = 1.18$
	Molecular weight:	$MW = 25.45$
	Throat temperature:	$T_t = 2{,}780$ K
	Density of product gases:	$\rho_p = 4.32$ kg/m^3
	Density of propellant:	$\rho_b = 1{,}720$ kg/m^3
	Burning rate (at $1{,}013 \times 10^5$ Pa):	$r = 0.847$ cm/s
	Chamber temperature:	$T_o = 3{,}000$ K
	Chamber pressure:	$P_o = 6.9$ MPa
	Atmospheric pressure:	$P_3 = 0.1013$ MPa

Assumed geometry:

Initial distance between propellant and top surface of chamber: $h = 1.91$ cm

Propellant web thickness: $b = 1.27$ cm

Length of propellant upstream of burning rate measurement: $L = 25.4$ cm

Required crossflow velocity for M = 1.0:

$$V = M \sqrt{\frac{kR_u T}{MW}}$$

$$= 1.0 \sqrt{\frac{(1.18)(8{,}314 \text{ J/kmol K})(2780 \text{ K})}{25.45 \text{ kmol/kg}}} = 1{,}035 \text{ m/s}$$

Velocity resulting from combustion of propellant in test section:

$$m_P = \rho_b A_b r = \rho_P V_P A$$

$$V_P = \frac{\rho_b}{\rho_P}\frac{L}{h} r = \left(\frac{1720 \frac{kg}{m^3}}{4.32 \frac{kg}{m^3}}\right)\left(\frac{25.4 \text{ cm}}{1.9 \text{ cm}}\right)\left(0.84 \text{ cm/s}\right)\left(\frac{1\text{m}}{100 \text{ cm}}\right)$$

$$V_P = 44.7 \text{ m/s}$$

Percentage of required crossflow velocity supplied by the test section:

$$\%V = \frac{V_P}{V} \times 100\% = \frac{44.7}{1035} \times 100\% = 4.3\%$$

Required mass flow for M = 1.0:

$$m = m_D + m_P = \rho_D V_D A + \rho_P V_P A$$

Assuming $\rho_D = \rho_P$: $m = \rho A(V_D + V_P)$

$$m = (4.32 \text{ kg/m}^3)(1035 \text{ m/s})A$$

$$m = 4{,}471A \frac{kg}{s} \quad (A \text{ in } m^2)$$

$$m = 0.447A \frac{kg}{s} \quad (A \text{ in } cm^2)$$

Requiring the mass flow not to exceed 4.3 kg/s, the flow area is:

$$A = \left(4.3 \frac{kg}{s}\right)\left(\frac{s}{0.447 \text{ kg}}\right) m^2$$

$$A = 9.62 \text{ cm}^2$$

Estimate of boundary layer thickness:

$$\delta_2 = \frac{0.036\nu^{0.2}}{u_\infty^{3.29}} \left[u_\infty^{3.86} \, x \right]^{0.8}$$

$$\frac{\delta}{\delta_2} = 10.31$$

The boundary layer will be thickest for low velocities.

For M = 0.2:

$$\delta_2 = \frac{(0.036)(240 \times 10^{-6} \text{ m}^2/\text{s})^{0.2}}{(207 \text{ m/s})^{3.29}} \cdot \left[(207 \text{ m/s})^{3.86} \, (0.254 \text{ m}) \right]^{0.8}$$

$$\delta_2 = 7.73 \times 10^{-4} \text{ m}$$

$$\delta = 10.31 \, (7.73 \times 10^{-4} \text{ m}) = 0.8 \text{ cm}$$

At burnout the crossflow velocity will be:

$$V_b = \frac{m}{\rho_P A} = \frac{4.3 \frac{kg}{s} \left(\frac{100cm}{m}\right)^2}{(6.73\ kg/m^3)(4.40\ cm)(5.06\ cm)} = 287\ m/s$$

$$M = \frac{287}{1035} = 0.28$$

Initial thrust (M=1.0):

For k = 1.2, M = 1: $\frac{P}{P_0} = 0.5644$

$$P_2 = (0.5644)(6.90 \times 10^6\ Pa)$$

$$P_2 = 3.89 \times 10^6\ Pa$$

$$F = (1035\ m/s)(4.3\ kg/s) + (3.89 \times 10^6 - 1.013 \times 10^5)(Pa)(9.62\ cm^2)\left(\frac{m}{100cm}\right)^2$$

F = 8.10 kN

Final thrust (M = 0.59):

$$\frac{P_2}{P_0} = 0.955 \qquad P_2 = 6.58 \times 10^6$$

$$F = (4.3\ kg/s)(287\ m/s) + (6.58 \times 10^6 - 1.013 \times 10^5)(Pa)(22.26\ cm^2)\left(\frac{m}{100cm}\right)^2$$

F = 15.7 kN

Estimate of augmentation ratio, r/r_o, using Lenoir and Robillard model:

$$r = r_o + r_e = r_o + \alpha G^{0.8} L^{-0.2} \exp\{-\beta r \rho_b / G\}$$

From the work of Lenoir and Robillard:

$$\alpha = 1.521 \times 10^{-5} \frac{m^{2.8}}{kg^{0.8} s^{0.2}}$$

$$\beta = 53$$

For M = 1:

$$r = 0.709 + \left[1.521 \times 10^{-5} \frac{m^{2.8}}{kg^{0.8} s^{0.2}}\right] \cdot \left[(4.32 \text{ kg/m}^3)(1033 \text{ m/s})\right]^{0.8} \cdot [0.254 \text{ m}]^{-0.2} \exp\{-53(1720)r/(4.32)(1033)\}$$

$$r = 0.709 + 1.663 \exp[-0.204 r] \quad \text{(cm/s)}$$

$$r = 1.85 \text{ cm/s}$$

$$r/r_o = 2.6$$

Similarly, at burnout, for M = 0.2:

$$r/r_o = 1.55$$

Required surface area of propellant in driver motor:

$$m = \rho_b A_b r$$

$$A_b = \frac{m}{\rho_b r} = \frac{(4.3 \text{ kg/s})}{\left(1{,}720 \frac{\text{kg}}{\text{m}^3}\right)\left(0.84 \frac{\text{cm}}{\text{s}}\right)\left(\frac{1\text{m}}{100 \text{ cm}}\right)} = 0.298 \text{ m}^2$$

Required length of driver for a single perforation 25.4 cm in diameter:

$$A_b = \pi d L$$

$$L = \frac{A_b}{\pi d} = \frac{(0.298 \text{ m}^2)}{\pi \text{ (25.4 cm)}\left(\frac{1\text{m}}{100 \text{ cm}}\right)} = 0.373 \text{ m}$$

$$L = 37.3 \text{ cm}$$

The vita has been removed from the scanned document